# Supplementary Information

## Design of Monolithic Closed-Cell Polymer Foams via Controlled Gas-Foaming for High-Performance Solar-Driven Interfacial Evaporation

Lifang Qiao, Na Li, Lin Luo, Jintao He, Yuxuan Lin, Jingjing Li, Liangmin Yu, Cui Guo,* Petri Murto* & Xiaofeng Xu*

* Corresponding authors: X. Xu, email: xuxiaofeng@ouc.edu.cn
P. Murto, email: pm707@cam.ac.uk
C. Guo, email: guocui@ouc.edu.cn

## Table of Contents

## 1. Materials

PAN ($M_w$ = 150.0 kDa) was purchased from Hefei Sipin Technology Co., Ltd, China. BPA prepolymer was purchased from Aladdin Chemical Co., Ltd., China. $NaBH_4$, DMF and methanol were purchased from Sinopharm Chemical Reagent Co., Ltd, China.

## 2. Materials characterization

The morphologies and elemental mapping were characterized by a scanning electron microscope (VEGA3, TESCAN) in combination with energy dispersive X-ray spectrometry. 3D optical microscope images were characterized via a 3D laser scanning confocal microscope (VK-X260K, Keyence). Contact angles were measured via a contact angle goniometer (JC2000DM, Powereach) by using 4 μL of water droplet as an indicator. The FTIR spectra were recorded via a Nicolet FTIR infrared microscope (iS50 FT-IR, Thermo Fisher Scientific). The density of all samples was measured and calculated by a high-precision foam density tester (AU-120PF, Quarrz, accuracy: 0.1 mg $cm^{-3}$). The tensile and compressive tests were performed using a universal mechanical testing system equipped a 100 N digital force gauges (M5-100, Mark-10, accuracy: 0.02 N) and a force test stand (ESM 303, Mark-10). The reflectance spectra were measured via a UV−Vis−NIR spectrometer (Lambda 950, PerkinElmer) equipped with an integrating sphere. The absorptance at each wavelength is defined by $1 - T - R$, where T and R are the corresponding transmittance and reflectance, respectively. Thermal conductivity was measured by a homemade thermal conductivity testing system. Specific surface areas were measured by $N_2$ adsorption at 77 K (Tristar II 3020, Norcross) and calculated by using Brunauer-Emmett-Teller (BET) equation. Biofouling characterization of the foams was performed via a CytoFLEX flow cytometer (A00-1-1102, Beckman Coulter), and the data collection and analysis were conducted by using CytExpert software. Biofouling characterization of the films was performed via a confocal laser scanning microscopy (Nikon A1, Japan). ImageJ software was used to analyze the CLSM images.

## 3. SEM images

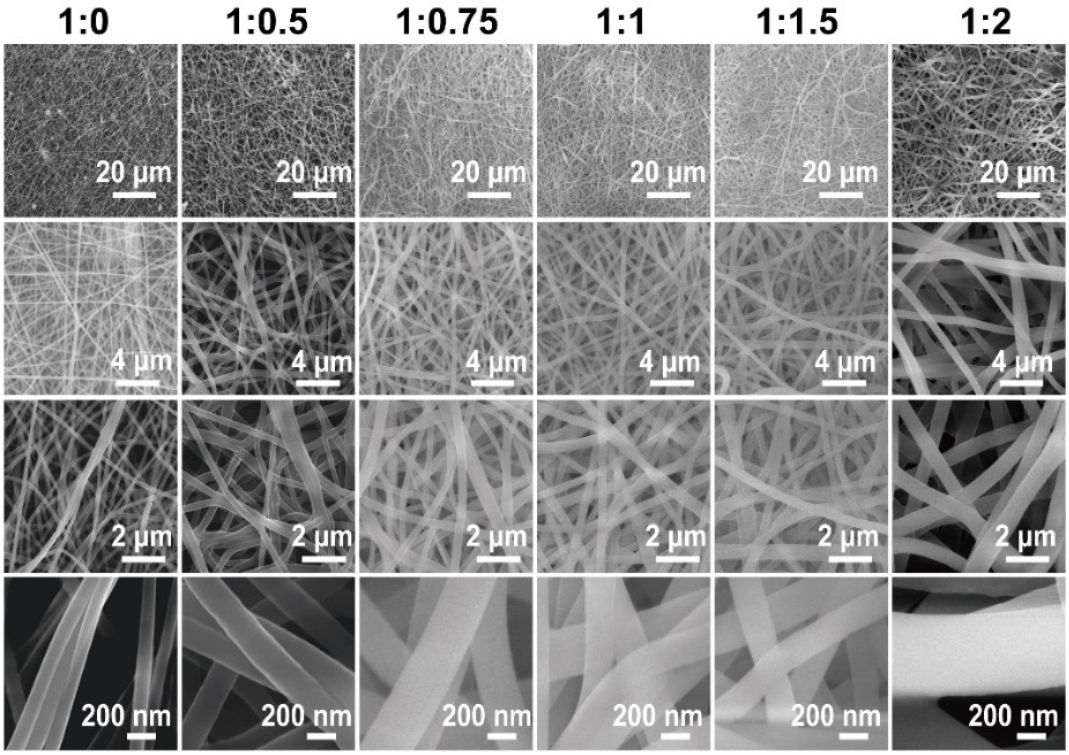


**Figure S1.** SEM images of 2D nanofibrous membranes with different loading of PAN and BPA epoxy resins.

## 4. Diameter distribution

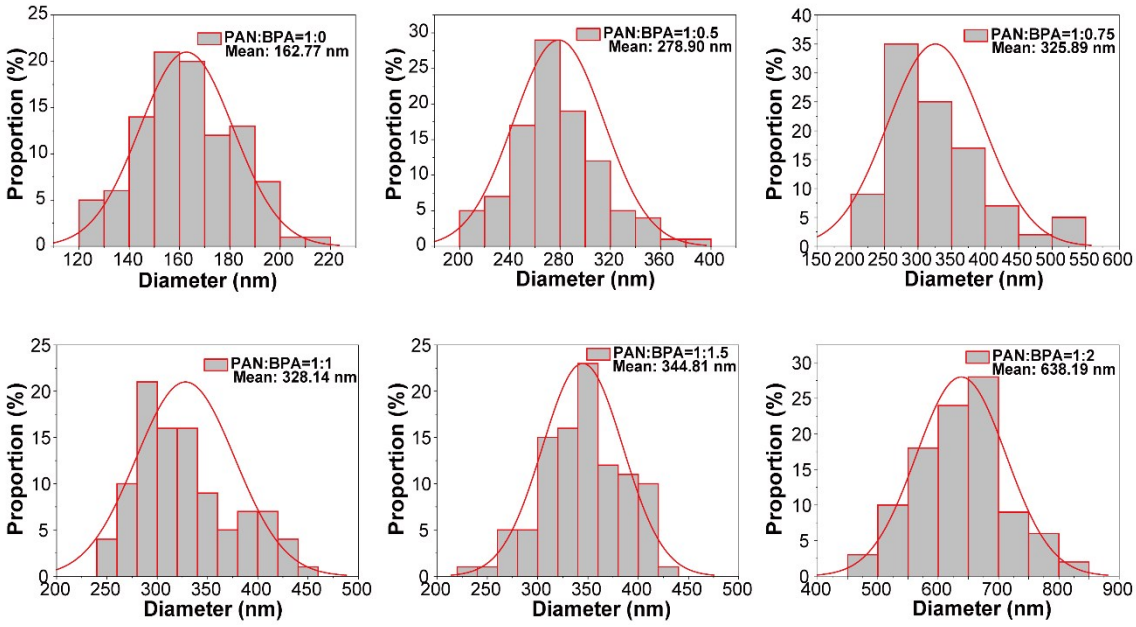


**Figure S2.** Diameter distribution and mean diameter of 2D nanofibrous membranes with different loading of PAN and BPA epoxy resins.

## 5. EDS mapping

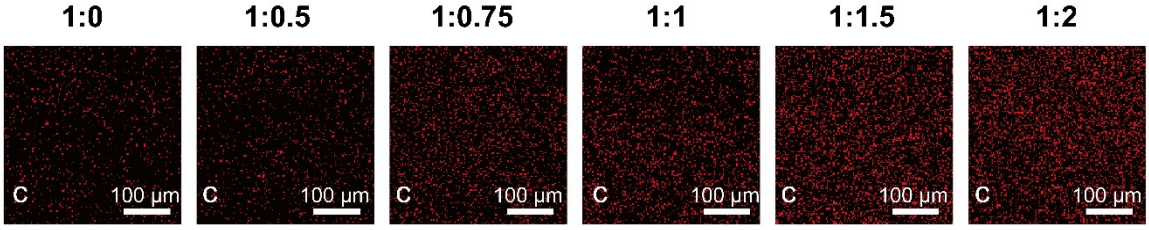


**Figure S3.** EDS mapping of carbon (C) of 2D nanofibrous membranes with different loading of PAN and BPA epoxy resins.

## 6. Atomic percentage of elements

**Table S1.** Atomic percentage of C, N and O in 2D nanofibrous membranes with different loading of PAN and BPA epoxy resins.

| element | C (%) | N (%) | O (%) |
|---|---|---|---|
| 1:0.5 | 46.9 | 30.0 | 23.1 |
| 1:0.75 | 51.8 | 27.6 | 20.6 |
| 1:1 | 49.0 | 28.5 | 22.5 |
| 1:1.5 | 47.0 | 25.4 | 27.6 |
| 1:2 | 47.3 | 21.5 | 31.2 |

## 7. FTIR spectra

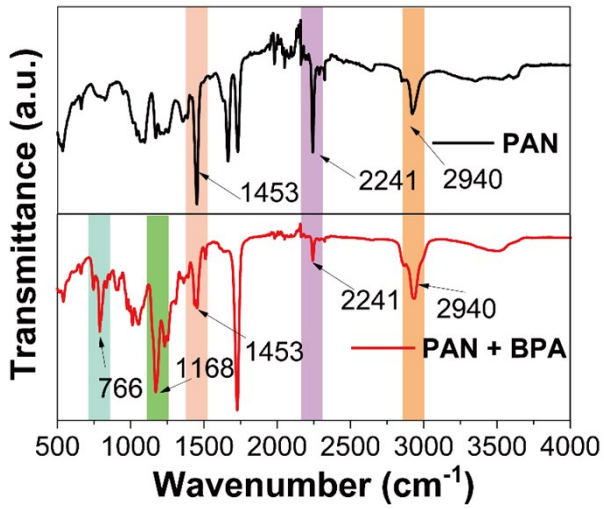


**Figure S4.** FTIR spectra of neat PAN and PAN/BPA composite membranes.

## 8. Water contact angle measurements

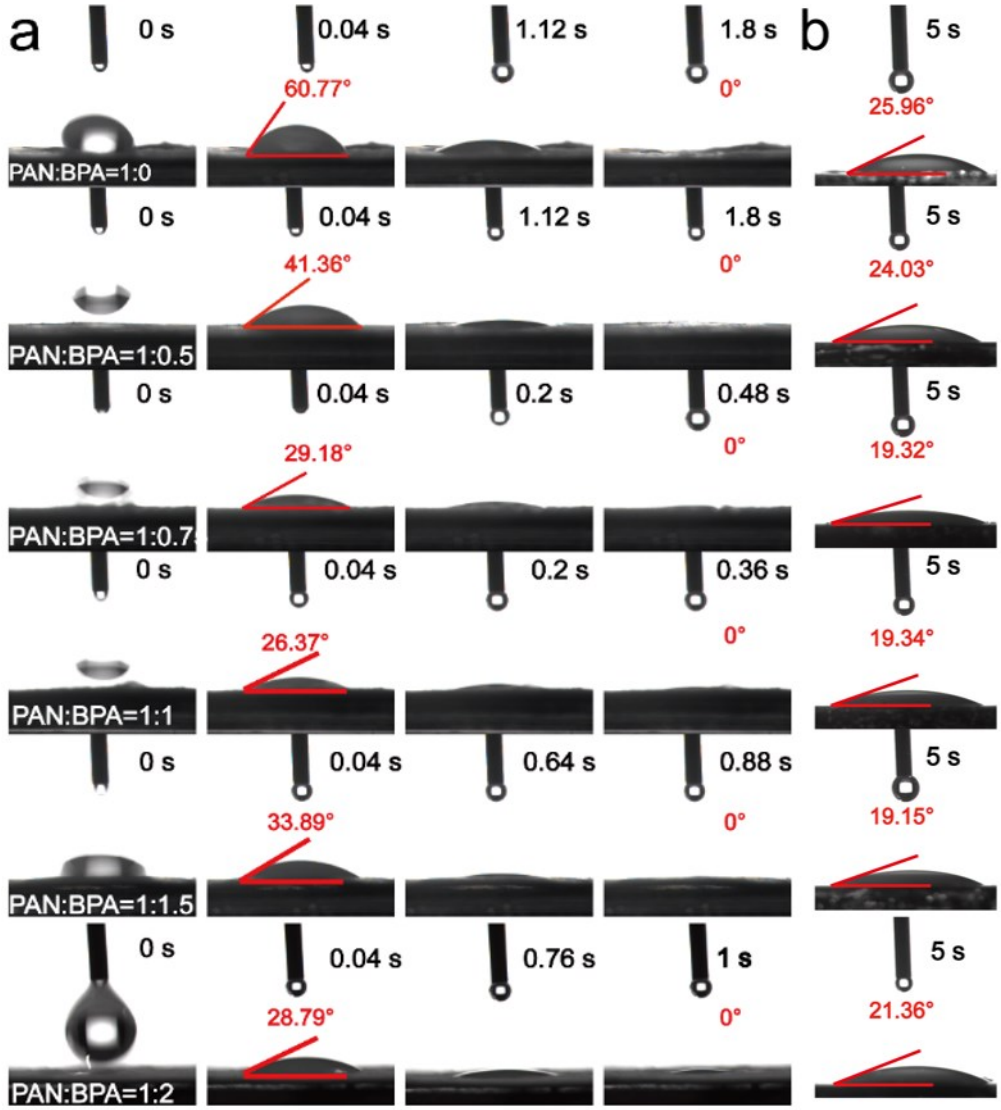


**Figure S5. (**a) Time-lapse snapshots of water droplet absorption through 2D nanofibrous membranes with different loading of PAN and BPA epoxy resins; (b) water contact angles on thin films with different loading of PAN and BPA epoxy resins.

## 9. Tensile testing

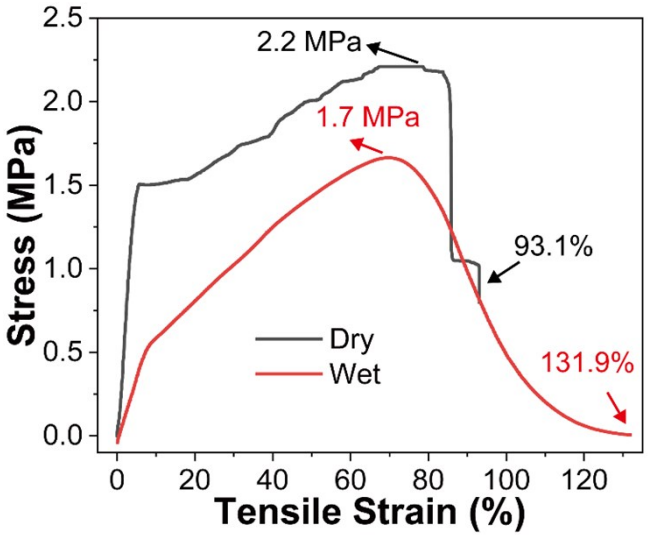


**Figure S6.** Tensile stress−strain curves of the PAN/BPA (1:1) nanofibrous membranes in dry and wet states.

## 10. Morphology of 3D composite foams

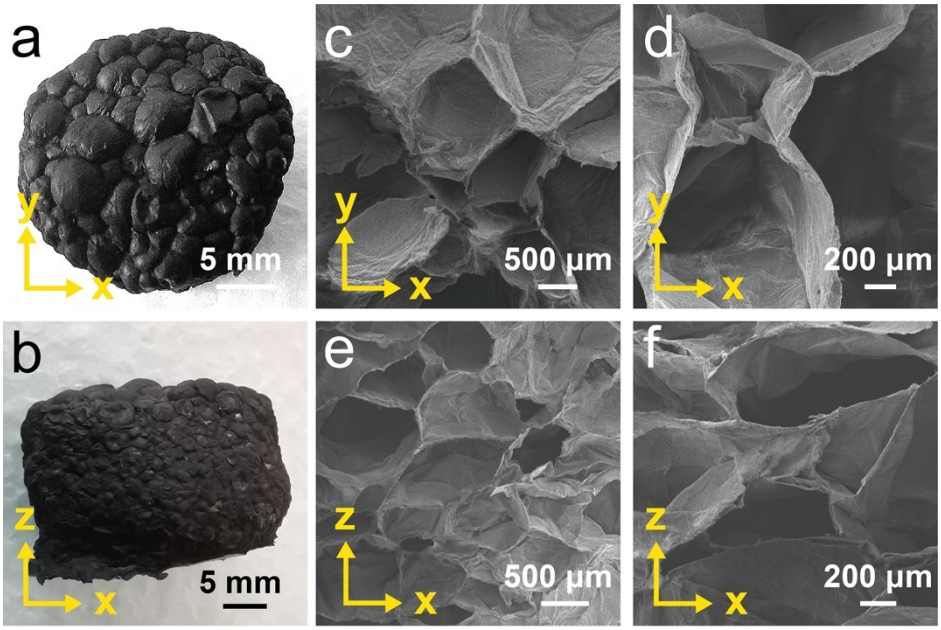


**Figure S7.** Digital photographs of a 3D composite foam (PAN:BAP = 1:1) (a) top view and (b) side view. SEM images of a 3D composite foam (PAN:BAP = 1:1) (c) and (d) transverse cross-sections; (e) and (f) longitudinal cross-sections.

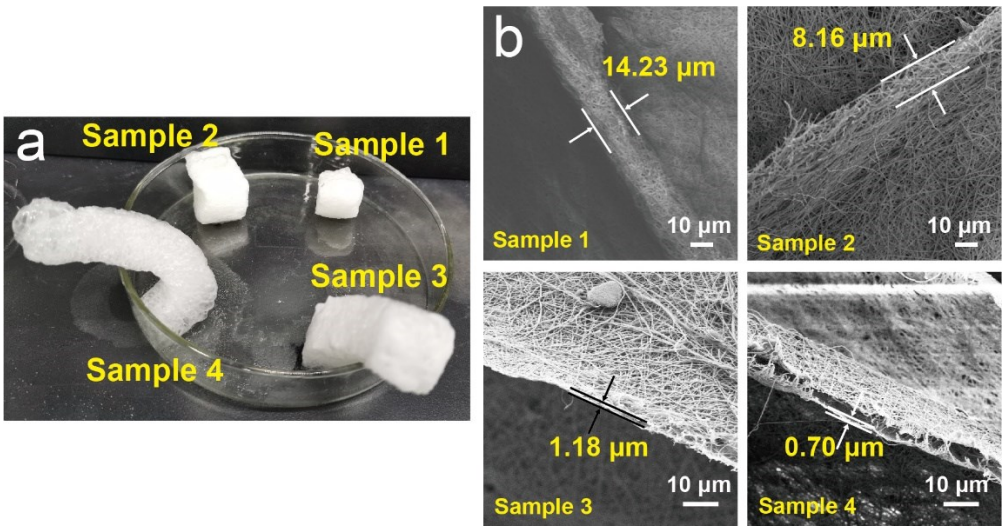


**Figure S8.** (a) Digital photographs of PAN:BPA (1:1) foams that gas-foamed by using different concentrations of $NaBH_4$ (Sample 1: 0.006 mol/cm$^2$; Sample 2: 0.02 mol/cm$^2$; Sample 3: 0.06 mol/cm$^2$ and Sample 4: 0.18 mol/cm$^2$); (b) corresphonding wall thickness of the foams.

## 11. Density of dry 3D foams

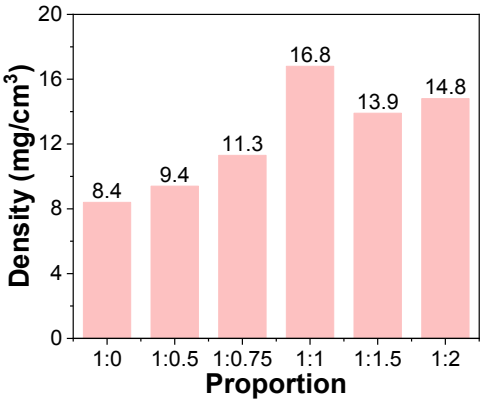


**Figure S9.** Density of 3D dry foams with different loading of PAN and BPA epoxy resins.

## 12. Compressive testing of 3D foams

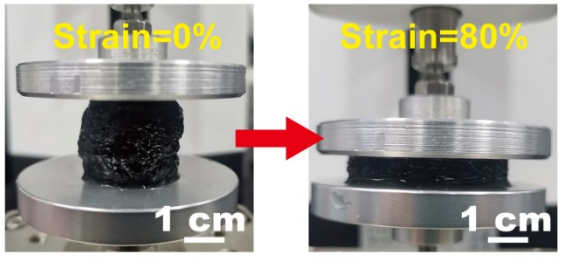


**Figure S10**. A digital photograph of compressive testing.

## 13. Artificial optical setup of evaporation measurements


**Figure S11**. A schematic diagram of the artificial optical setup for water evaporation measurements.

## 14. Summary of water evaperation rates

**Table S2**. Summary of materials, water evaporation rates and device configuration of interficial steam generators using PAN as structural elements.

| materials | evaporation rates ($kg\ m^{-2}\ h^{-1}$) | type | references |
|---|---|---|---|
| PAN/Nylon 6/PS/CB | 1.24 | indirect contact | 1 |
| CB/PMMA/PAN | 1.30 | direct contact | 2 |
| CB/PAN/PVDF | 1.20 | direct contact | 3 |
| RGO/cotton/PAN | 1.47 | direct contact | 4 |
| CNT/$MoS_2$/PAN | 1.44 | direct contact | 5 |
| PAN/rGO/PS | 1.46 | indirect contact | 6 |
| PAN/PVA/AuNR | 2.70 | direct contact | 7 |
| Co-Zn ZIF/$MoS_2$/PAN | 1.39 | direct contact | 8 |
| $SiO_2$ / MWCNTs-COOH / PAN/PS | 1.28 | indirect contact | 9 |
| PAN/GO | 2.27 | direct contact | 10 |

**Table S3**. Summary of materials, water evaporation rates and device configuration of interficial steam generators based on polymric sponges/foams.

| material | evaporation rate ($kg\ m^{-2}\ h^{-1}$) | type | references |
|---|---|---|---|
| Alkalized loofah sponge/carbonized loofah sponge | 1.36 | indirect contact | 11 |
| SnSe−$SnSe_2$/glassy carbon foam | 1.28 | direct contact | 12 |
| Carbonized loofah/hydrophilic loofah | 1.42 | direct contact | 13 |
| $Ni_1Co_3$@PDA/commercial sponge/sodium alginate | 2.42 | indirect contact | 14 |
| Konjac Glucomannan/rGO | 1.60 | direct contact | 15 |
| plant-derived carbon Nanospheres/polyvinyl alcohol sponge | 1.53 | direct contact | 16 |
| Carbonized towel-gourd sponges | 1.46 | indirect contact | 17 |
| Sodium alginate/M-PPy sponge | 1.48 | direct contact | 18 |
| $Fe_2O_3$/CNT/Ni nanocomposite foam | 1.48 | direct contact | 19 |
| Porous carbon foam (SPCF) | 1.48 | direct contact | 20 |
| Melamine foam | 1.476 | indirect contact | 21 |
| $Cu_xS$/Cu foam | 1.96 | indirect contact | 22 |
| $Cu_7S_4$-$MoS_2$-Au nanoparticles (CMA NPs)/PDMS | 3.82 | direct contact | 23 |
| CNT/CNC/PCC sponge/TE module | 1.36 | indirect contact | 24 |
| Ti foam/cotton/polyurethane sponge | 1.79 | direct contact | 25 |
| Carbon foams (CFs) | 1.03 | direct contact | 26 |
| rGO foam | 2.40 | direct contact | 27 |
| rGO/cotton fabric/ VOPPF | 1.47 | direct contact | 4 |
| GS | 1.118 | direct contact | 28 |
| AMS | 1.98 | indirect contact | 29 |
| PBP/$Bi_2S_3$/PU | 1.66 | direct contact | 30 |
| PFS/rGO | 1.38 | direct contact | 31 |
| CS | 1.39 | direct contact | 32 |
| Polyurethane sponge/dopamine hydrochloride | 0.83 | direct contact | 33 |

## 15. Morphology of 3D composite hydrogels

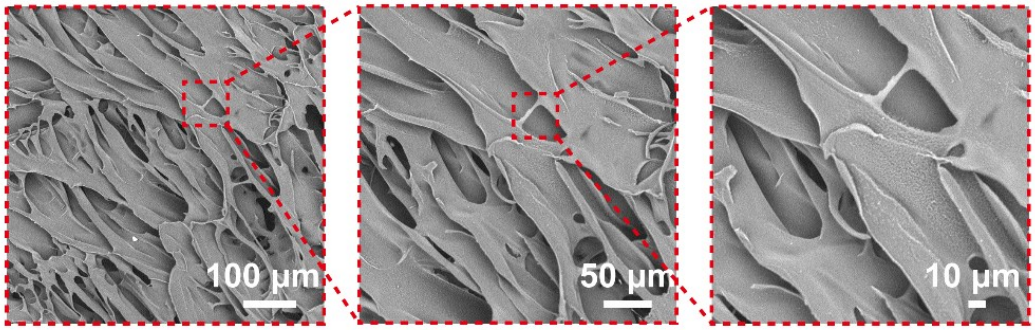


**Figure S12**. Cross-sectional SEM images of the 3D composite hydrogels (PAN:BPA=1:1).

## 16. Water diffusion

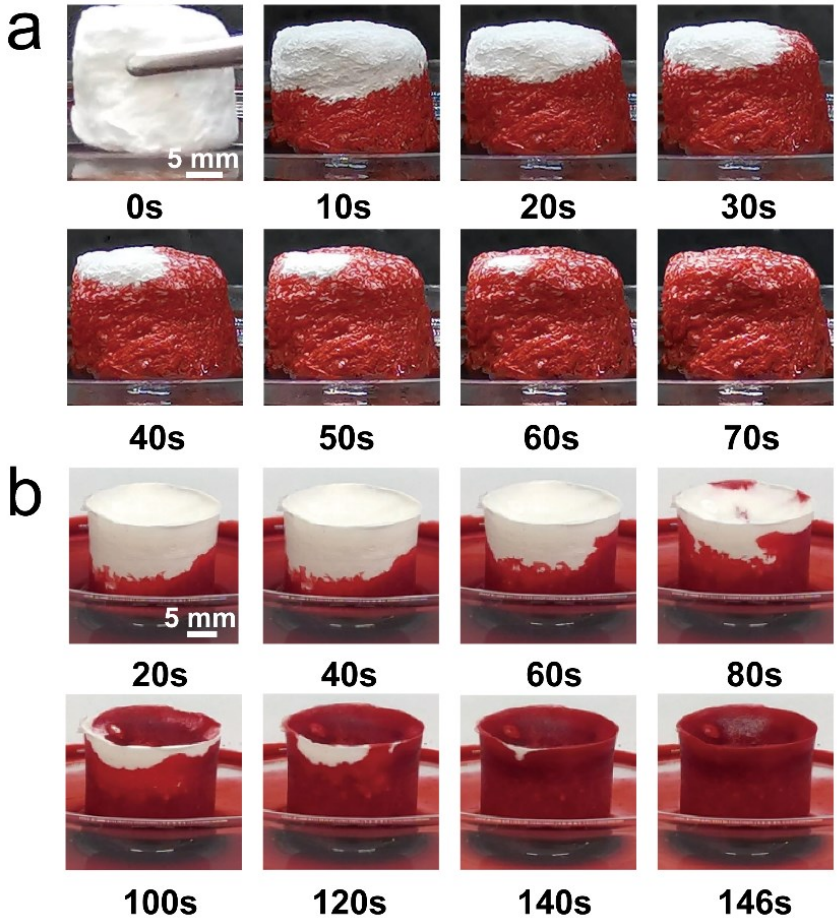


**Figure S13**. Water diffusion characterization of (a) 3D foam and (b) hydrogel based on PAN/BPA (1:1) composites (all samples have similar height of ~1.5 cm).

## 17. Thermal conductivity measurements

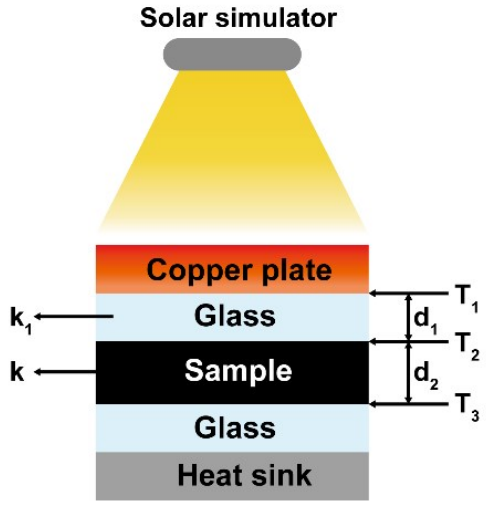


**Figure S14**. A schematic diagram of thermal conductivity measurements.

The thermal conductivities of PAN/BPA sponge and hydrogel were measured via an IR imaging method[34]. The samples with thickness of ~3.5 mm was sandwiched between two 1.1 mm glasses. The sandwich structure was placed between copper plate heated by solar simulator and heat sink. The heat transfer rate ($q$) permeating the sample can be calculated using the Fourier Equation S1:

$$q = -k_1\frac{T_2 - T_1}{d_1} = -k\frac{T_3 - T_2}{d_2} \quad \text{(S1)}$$

where $k_1$ is the thermal conductivity of glass (1.05 W $m^{-1}K^{-1}$)[35]. $T_1$, $T_2$, $T_3$ are the average temperatures at the interface of copper plate–top glass, top glass–sample, sample–bottom glass, respectively. The thermal conductivities of samples ($k$) can be calculated by Equation S1 based on IR images.

**18. Calculation of water evaporation rates and light-to-heat conversion efficiencies**

The water evaporation rate can be calculated by Equation S2,[36]

$$v = \frac{\Delta m}{A \times \Delta t} \quad \text{(S2)}$$

where Δm is the mass change of water (kg), A is the surface area of the evaporator ($m^2$), and Δt is the time (h).

**19. Heat loss characterization of SG3 and SG4**

(i) Radiation loss:

The radiation loss was analyzed by Stefan-Boltzmann Equation S4,

$$\Phi = \varepsilon A \sigma (T_1^4 - T_2^4) \quad \text{(S3)}$$

$\Phi$ is heat flux (W), $\varepsilon$ denotes emissivity (Supposing the evaporator has a maximum emissivity of 1), $A$ is evaporation surface area (3.70 $cm^2$ for SG3, 4.56 $cm^2$ for SG4), $\sigma$ represents the Stefan-Boltzmann constant ($\sigma$ = 5.670373×$10^{-8}$ W $m^{-2}$ $K^{-4}$), $T_1$ is the average surface temperature of the solar absorber after stable steam generation under one-sun illumination (316.1 K for SG3, 314.2 K for SG4). $T_2$ is the ambient temperature around the evaporator (309.7 K). Therefore, based on Equation S3, we can calculate that the radiation heat loss of SG3 is ~3.08%. The radiation heat loss of SG4 is ~1.7%.

(ii) Conduction loss:

The heat loss of convection was analyzed according to the following Equation S5.

$$Q = Cm\Delta T \quad \text{(S4)}$$

$Q$ denotes the heat energy, $C$ is the specific heat capacity of pure water (4.2 kJ °$C^{-1}$ $kg^{-1}$), $m$ represents the weight of bulk water and $\Delta T$ is the increased temperature of the bulk water after stable steam generation. In our experimental, $m$ = 50 g, $\Delta T$ = 0.9 °C for SG3, $\Delta T$ = 0.4 °C for SG4. Therefore, based on Equation S4, we can calculate that the conduction heat loss of SG3

is ~14.1%. The conduction heat loss of SG4 is ~5.1%.

(iii) Convection loss:

The convection loss was calculated by Newton's law of cooling.

$$Q = hA\Delta T \qquad \text{(S5)}$$

$Q$ is the heat energy, $h$ denotes the convection heat transfer coefficient (~5 W $m^{-2}K^{-1}$)[37]. $A$ represents surface area. $\Delta T$ is difference between the ambient temperature around the evaporator and the surface temperature of the evaporator. Therefore, based on Equation S5, we can calculate that the convection heat loss of SG3 is ~2.2%. The convection heat loss of SG4 is ~1.25%.

(iv) Reflection loss:

The solar absorption of solar absorber is 94%; thus, the refection loss is ~6%.

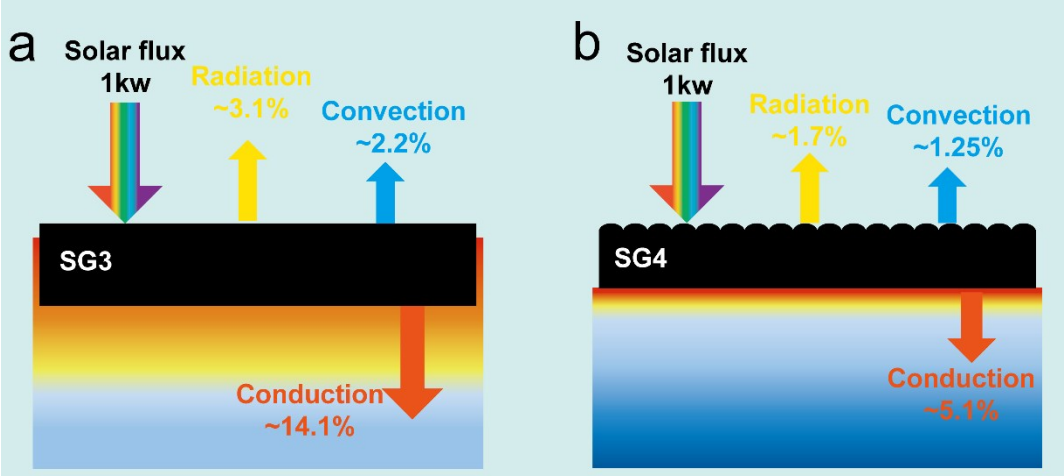


**Figure S15**. Energy balance and heat loss diagrams of (a) SG3 and (b) SG4.

## 20. Evaporation of SG4 in a wide range of pH

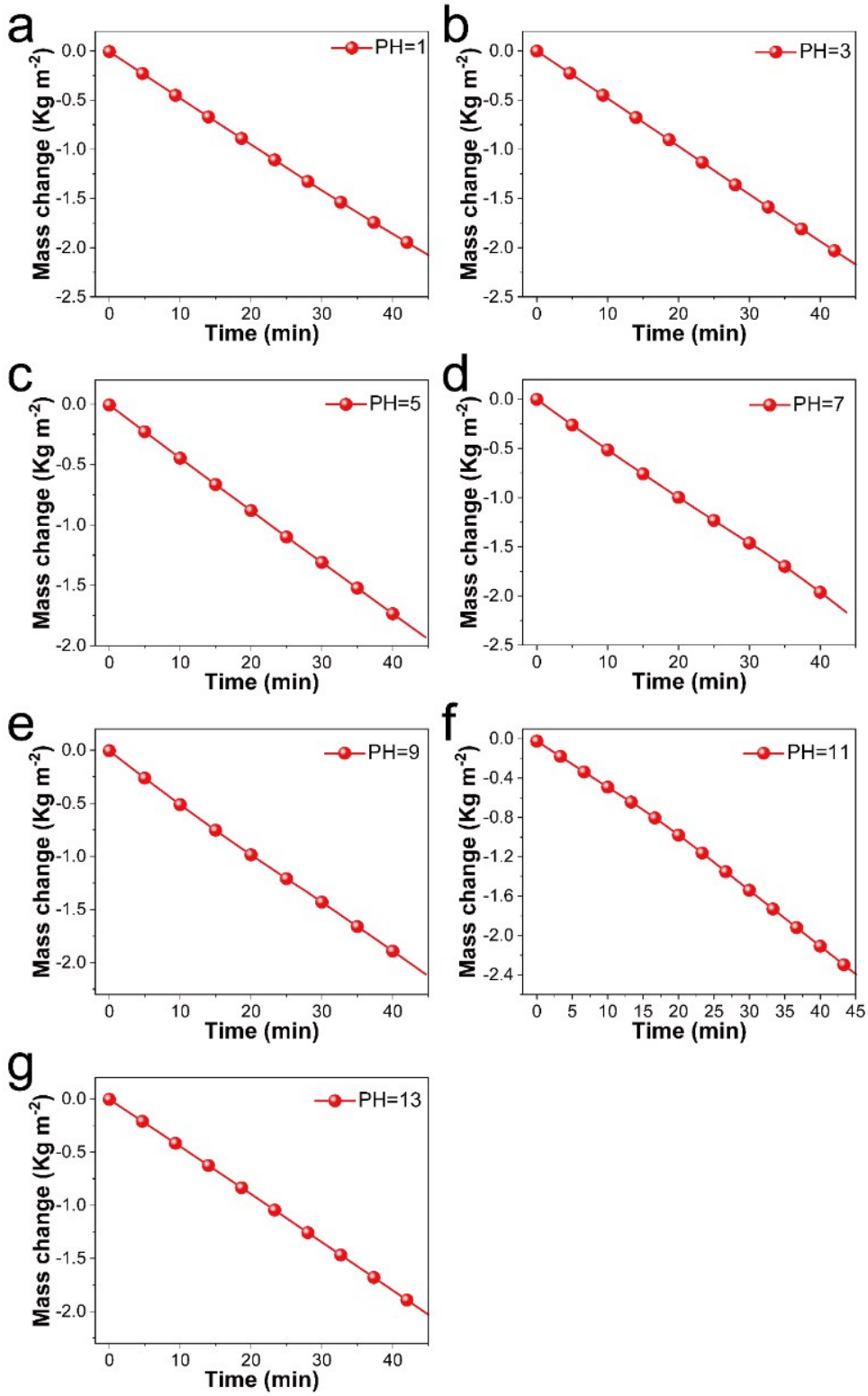


**Figure S16**. Mass changes of water over 40 min in different pH under one sun.

## 21. Evaporation of SG4 in different salinity

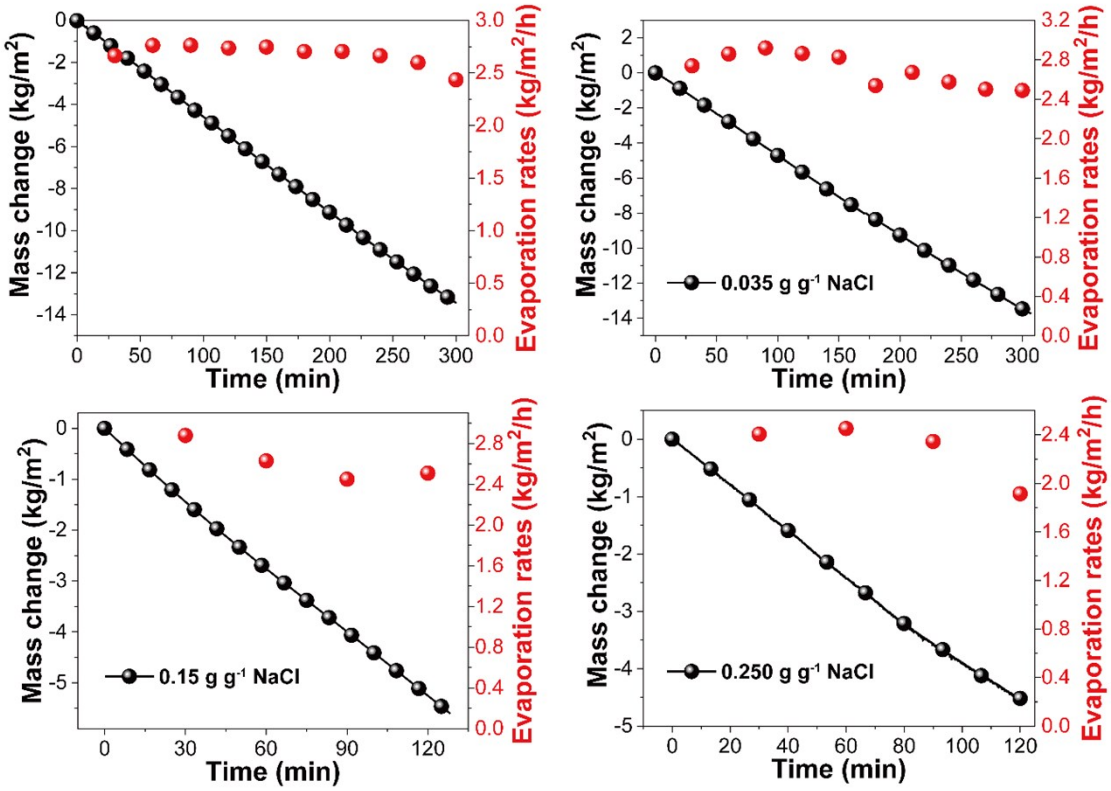


**Figure S17**. Mass changes of brine and evaperation rates over time in different salinity under one sun.

## 22. Evaporation of SG4 in outdoor measurements

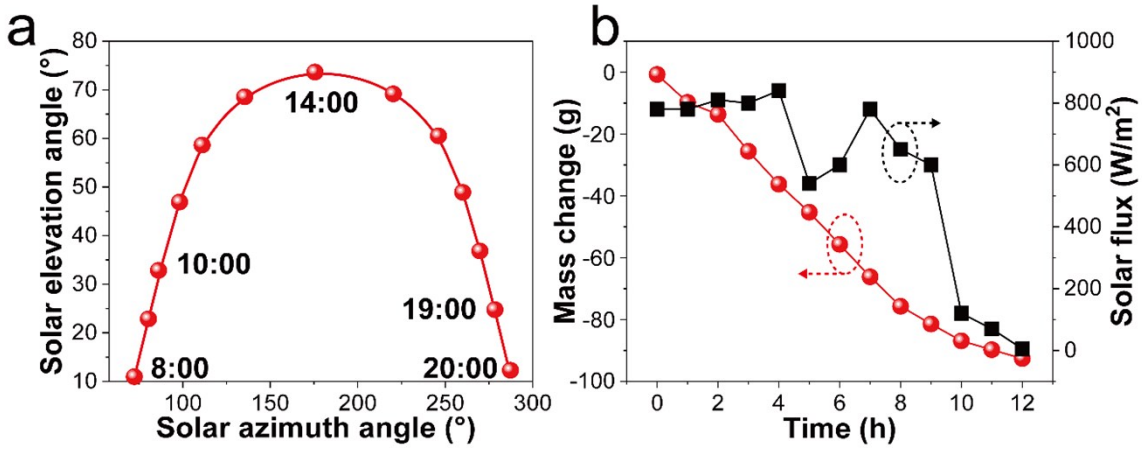


**Figure S18**. (a) Solar azimuth angle and solar elevation angle in real time; (b) Mass change and solar flux of SG4 during outdoor water evaporation measurements.

## 23. Salinity and TDS measurements

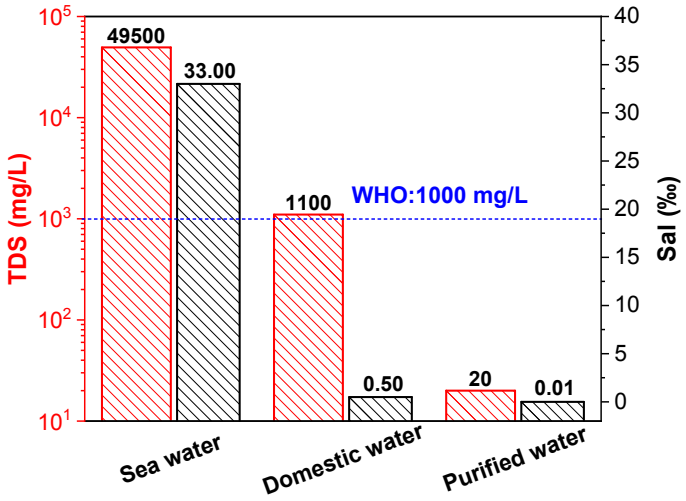


**Figure S19**. Salinity and TDS measurements for outdoor solar desalination.

## 24. Specific surface areas

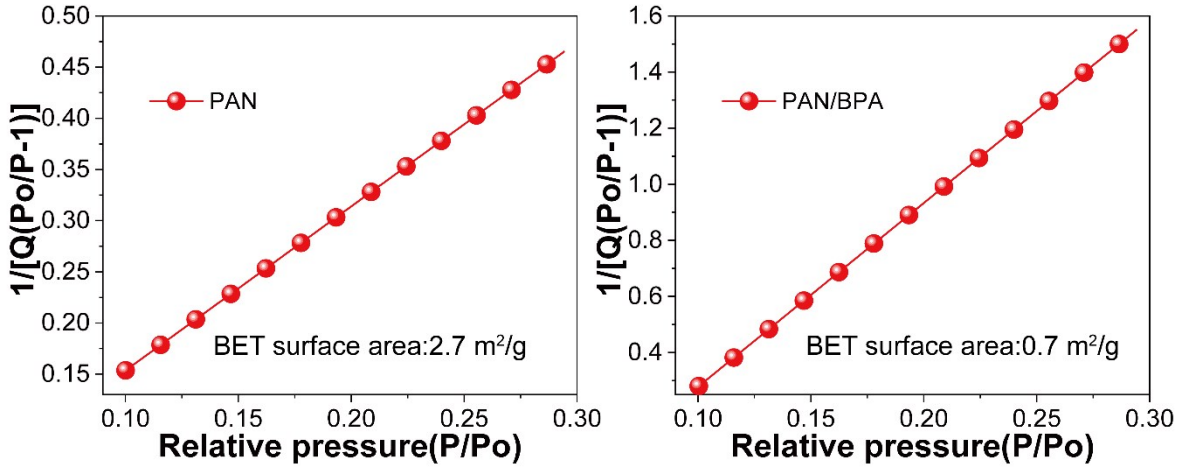


**Figure S20**. Characterization of BET specific surface areas of the 2D nanofibrous membranes based on neat PAN and PAN:BPA (1:1).

**25. Durability tests of 3D foams**

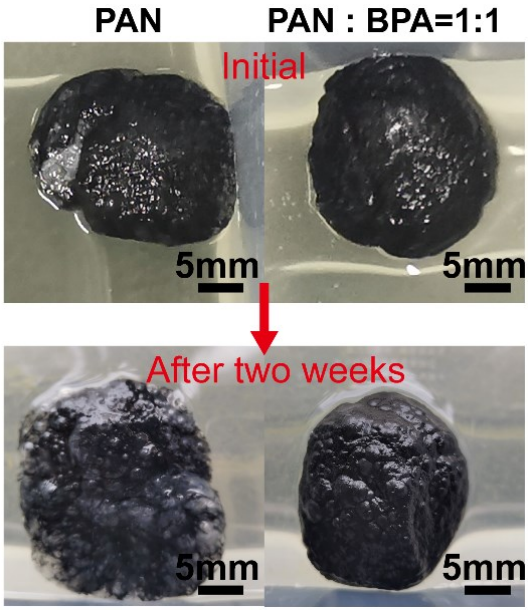


**Figure S21**. Digital photographs of neat PAN and PAN:BPA (1:1) foams before and after two weeks' soaking in natrual water.

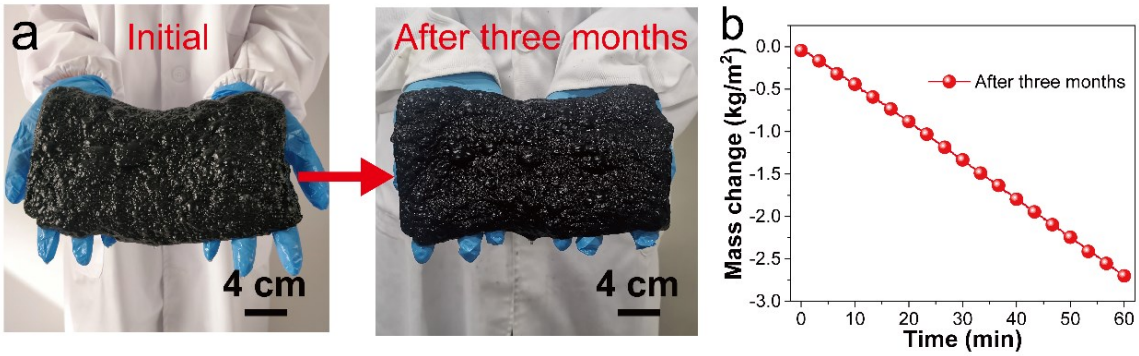


**Figure S22**. Didital photographs of a large-area PAN:BPA (1:1) foam before and after three months' soaking in natural water; (b) corresphonding mass change of water during solar evaperation.

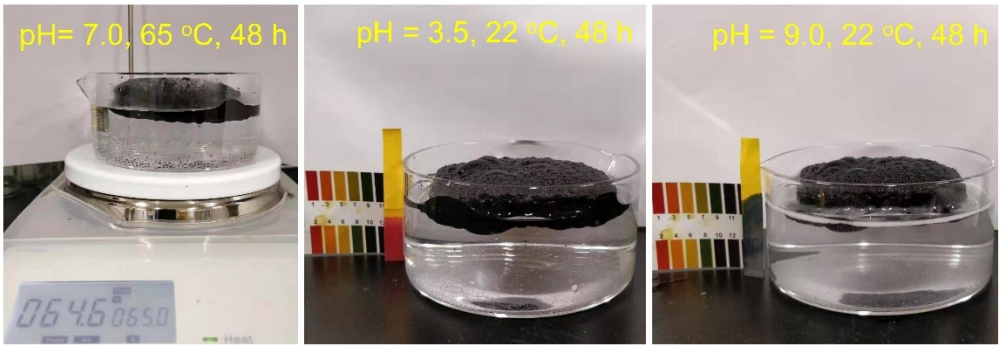


**Figure S23**. Digital photographs of PAN:BPA (1:1) foams after soaking in warm, acidic and alkaline water.

## 26. References


1. Y. Jin, J. Chang, Y. Shi, L. Shi, S. Hong and P. Wang, *J. Mater. Chem. A*, 2018, **6**, 7942-7949.
2. W. Xu, X. Hu, S. Zhuang, Y. Wang, X. Li, L. Zhou, S. Zhu and J. Zhu, *Adv. Energy Mater.*, 2018, **8**, 1702884.
3. T. Gao, Y. Li, C. Chen, Z. Yang, Y. Kuang, C. Jia, J. Song, E. M. Hitz, B. Liu, H. Huang, J. Yu, B. Yang and L. Hu, *Small Methods*, 2019, **3**, 1800176.
4. Q. Zhang, H. Yang, X. Xiao, H. Wang, L. Yan, Z. Shi, Y. Chen, W. Xu and X. Wang, *J. Mater. Chem. A*, 2019, **7**, 14620-14628.
5. B. Zhu, H. Kou, Z. Liu, Z. Wang, D. Macharia, M. Zhu, B. Wu, X. Liu and Z. Chen, *ACS Appl. Mater. Interfaces*, 2019, **11**, 35005-35014.
6. X. Fan, B. Lv, Y. Xu, H. Huang, Y. Yang, Y. Wang, J. Xiao and C. Song, *Solar Energy*, 2020, **209**, 325-333.
7. Z. Huang, S. Li, X. Cui, Y. Wan, Y. Xiao, S. Tian, H. Wang, X. Li, Q. Zhao and C. Lee, *J. Mater. Chem. A*, 2020, **8**, 10742-10746.
8. H. Peng, L. Zhang, M. Li, M. Liu, C. Wang, D. Wang and S. Fu, *Chem. Eng. J.*, 2020, **397**, 125410.
9. Q. Qi, W. Wang, Y. Wang and D. Yu, *Sep. Purif. Technol.*, 2020, **239**, 116595.
10. L. Wang, C. Liu, H. Wang, Y. Xu, S. Ma, Y. Zhuang, W. Xu, W. Cui and H. Yang, *ACS Appl. Mater. Interfaces*, 2020, **12**, 24328-24338.
11. Y. Lu, X. Wang, D. Q. Fan, H. Yang, H. L. Xu, H. H. Min and X. F. Yang, *Sustain. Mater. Technol.*, 2020, **25**, e00180.
12. Z. Tahir, S. Kim, F. Ullah, S. Lee, J. Lee, N. Park, M. Seong, S. Lee, T. Ju, S. Park, J. Bae, J. Jang and Y. Kim, *ACS Appl. Mater. Interfaces*, 2020, **12**, 2490-2496.
13. C. Liu, K. V. Hong, X. Sun, A. Natan, P. C. Luan, Y. Yang and H. L. Zhu, *J. Mater. Chem. A*, 2020, **8**, 12323-12333.
14. B. Shao, Y. D. Wang, X. Wu, Y. Lu, X. F. Yang, G. Y. Chen, G. Owens and H. L. Xu, *J. Mater. Chem. A*, 2020, **8**, 11665-11673.
15. K. Yu, P. Shao, P. Meng, T. Chen, J. Lei, X. F. Yu, R. He, F. Yang, W. K. Zhu and T. Duan, *J. Hazard. Mater.*, 2020, **392**, 122350.
16. H. M. Wilson, Tushar, S. R. Ar and N. Jha, *Sol. Energy Mater. Sol. Cells*, 2020, **210**, 110489.

17. X. L. Shan, A. Q. Zhao, Y. W. Lin, Y. J. Hu, Y. S. Di, C. H. Liu and Z. X. Gan, *Adv. Sustainable Syst.*, 2020, **4**, 1900153.
18. Y. K. Fan, W. Bai, P. Mu, Y. N. Su, Z. Q. Zhu, H. X. Sun, W. D. Liang and A. Li, *Sol. Energy Mater. Sol. Cells*, 2020, **206**, 110347.
19. S. Han, J. Yang, X. Li, W. Li, X. Zhang, N. Koratkar and Z. Yu, *ACS Appl. Mater. Interfaces*, 2020, **12**, 13229-13238.
20. C. Wang, J. Wang, Z. Li, K. Xu, T. Lei and W. Wang, *J. Mater. Chem. A*, 2020, **8**, 9528-9535.
21. S. Meng, X. Zhao, C. Tang, P. Yu, R. Bao, Z. Liu, M. Yang and W. Yang, *J. Mater. Chem. A*, 2020, **8**, 2701-2711.
22. W. Huang, P. Su, Y. Cao, C. Li, D. Chen, X. Tian, Y. Su, B. Qiao, J. Tu and X. Wang, *Nano Energy*, 2020, **69**, 104465.
23. H. Wang, R. Zhang, D. Yuan, S. Xu and L. Wang, *Adv. Funct. Mater.*, 2020, **30**, 2003995.
24. L. Zhu, T. Ding, M. Gao, C. K. Peh and G. W. Ho, *Adv. Energy Mater.*, 2019, **9**, 1900250.
25. K. Yin, S. Yang, J. R. Wu, Y. J. Li, D. K. Chu, J. He and J. A. Duan, *J. Mater. Chem. A*, 2019, **7**, 8361-8367.
26. P. Qiu, F. Liu, C. Xu, H. Chen, F. Jiang, Y. Li and Z. Guo, *J. Mater. Chem. A*, 2019, **7**, 13036-13042.
27. H. Liang, Q. Liao, N. Chen, Y. Liang, G. Lv, P. Zhang, B. Lu and L. Qu, *Angew. Chem. Int. Ed.*, 2019, **58**, 19041-19046.
28. Z. Zhang, P. Mu, J. He, Z. Zhu, H. Sun, H. Wei, W. Liang and A. Li, *Chemsuschem*, 2019, **12**, 426-433.
29. F. Gong, H. Li, W. B. Wang, J. G. Huang, D. W. Xia, J. X. Liao, M. Q. Wu and D. V. Papavassiliou, *Nano Energy*, 2019, **58**, 322-330.
30. H. Y. Cheng, X. H. Liu, L. X. Zhang, B. F. Hou, F. Yu, Z. X. Shi and X. B. Wang, *Solar Energy Mater. Solar Cells*, 2019, **203**, 110127.
31. T. J. Chen, S. Wang, Z. Z. Wu, X. D. Wang, J. Peng, B. H. Wu, J. Q. Cui, X. L. Fang, Y. Q. Xiec and N. F. Zheng, *J. Mater. Chem. A*, 2018, **6**, 14571-14576.
32. L. Zhu, M. Gao, C. N. Peh, X. Wang and G. Ho, *Adv. Energy Mater.*, 2018, **8**, 1702149.
33. S. Ma, C. Chiu, Y. Zhu, C. Tang, H. Long, W. Qarony, X. Zhao, X. Zhang, W. Lo and Y. Tsang, *Appl. Energy*, 2017, **206**, 63-69.
34. H. Li, Y. He, Y. Hu and X. Wang, *ACS Appl. Mater. Interfaces*, 2018, **10**, 9362-9368.
35. J. Wan, A. Fan, H. Yao and W. Liu, *Energ. Convers. and Manage.*, 2015, **96**, 605-612.
36. X. Q. Li, G. Ni, T. Cooper, N. Xu, J. L. Li, L. Zhou, X. Z. Hu, B. Zhu, P. C. Yao and J. Zhu, *Joule*, 2019, **3**, 1798-1803.
37. H. Ghasemi, G. Ni, A. M. Marconnet, J. Loomis, S. Yerci, N. Miljkovic and G. Chen, *Nat. Commun.*, 2014, **5**, 4449.